

Provided for non-commercial research and education use.
Not for reproduction, distribution or commercial use.



This article appeared in a journal published by Elsevier. The attached copy is furnished to the author for internal non-commercial research and education use, including for instruction at the authors institution and sharing with colleagues.

Other uses, including reproduction and distribution, or selling or licensing copies, or posting to personal, institutional or third party websites are prohibited.

In most cases authors are permitted to post their version of the article (e.g. in Word or Tex form) to their personal website or institutional repository. Authors requiring further information regarding Elsevier's archiving and manuscript policies are encouraged to visit:

<http://www.elsevier.com/authorsrights>



Contents lists available at ScienceDirect

International Journal of Rock Mechanics & Mining Sciences

journal homepage: www.elsevier.com/locate/ijrmms

Technical Note

A new failure mode chart for toppling and sliding with consideration of earthquake inertia force



G. Yagoda-Biran*, Y.H. Hatzor

Department of Geological and Environmental Sciences, Ben-Gurion University of the Negev, Beer-Sheva, Israel

ARTICLE INFO

Article history:

Received 5 October 2012

Received in revised form

25 April 2013

Accepted 28 August 2013

Available online 20 September 2013

1. Introduction

Rock slope failures involving single plane sliding or toppling have been studied extensively in the past. The problem has typically been formulated for the case of a block on an inclined plane. The model of a block on an inclined plane can help simulate many problems in rock slope engineering: it can be used to represent finite rock blocks formed by intersections of steeply inclined joints and shallowly inclined bedding planes and thus it can sometimes be used to simulate landslides or rock slides. The simplicity of the model and its attractive applicability calls for development of analytical solutions as these are quite useful in practice.

A block on an incline has four different possible modes of failure (Fig. 1): (1) static stability, (2) downslope sliding, (3) toppling and sliding simultaneously and (4) rotation and toppling. The failure mode is controlled by the geometry of both the block and the inclined plane, and the frictional resistance of the interface between them, the three of which are defined by three angles as follows (Fig. 1): δ , the block aspect angle defined by the ratio of the block width b and height h ; α , the inclination angle of the slope, will be referred to herein as the slope angle; and ϕ , the friction angle of the interface between the slope and the block. Any combination of these three angles will determine whether the block will move or not, and if so, what will be the mode of its first motion. Clearly, correct assessment of the failure mode is a prerequisite for correct risk assessment and sound support design.

Ashby [1] and Hoek and Bray [2] derived and plotted the modes of failure for the case of block on an incline in δ - α space using static limit equilibrium analysis (LEA). Static LEA implies finding

the forces acting on the block at a state of limiting equilibrium, namely, before imminent failure. Ashby's [1] and Hoek and Bray's [2] chart is presented in Fig. 2.

According to results of the static LEA performed by Ashby [1] and Hoek and Bray [2], when $\alpha < \phi$ the block will either be stable ($\delta > \alpha$) or topple ($\delta < \alpha$). When $\alpha > \phi$ the block will either slide ($\delta > \alpha$), or slide and topple simultaneously ($\delta < \alpha$). The original boundaries between those failure modes are assigned numbers here (Fig. 2); these numbers will be referred to herein when discussing failure mode boundaries.

Voegelé [3] compared the analytical results with distinct element method (DEM) simulations and discovered that in some cases while the block should have failed in sliding and toppling according to the mode chart in Fig. 2, in fact it experienced sliding alone when studied with DEM. Thus, he concluded that the Hoek and Bray [2] chart was too elementary to predict the exact dynamic behavior of slender blocks resting on an inclined plane.

Bray and Goodman [4] re-visited this problem and treated boundary 3 in Fig. 2 as a "dynamic" boundary. Their approach changed the condition for sliding to $\alpha > \phi$, and $\delta \geq \phi$ (Fig. 3). Yu et al. [5] later found that results of DEM simulations and physical models agree with Bray and Goodman's [4] modified chart.

Sagaseta [6] argued that Bray and Goodman's modification is correct but incomplete because at boundary 4 the state of equilibrium is dynamic rather than static; the derivation of the equilibrium equations for that boundary is provided in his paper. Yeung [7] studied this problem with the two dimensional Discontinuous Deformation Analysis method (2D-DDA, [8–11]) and compared his results to the chart published by Bray and Goodman [4]. He discovered that while 2D-DDA results agree with the first three boundaries, reassuring the modification of Bray and Goodman [4] to boundary 3, there is a discrepancy between the results obtained by 2D-DDA and the behavior predicted by boundary 4 in Bray and Goodman's chart. In some cases, while Bray and Goodman's chart predicts sliding and toppling, DDA

* Correspondence to: The Department of Geological and Environmental Sciences, Ben-Gurion University of the Negev, P.O. Box 653, 84105 Beer-Sheva, Israel. Tel.: +972 8 6477855; fax: +972 8 6472997.

E-mail address: birangony@gmail.com (G. Yagoda-Biran).

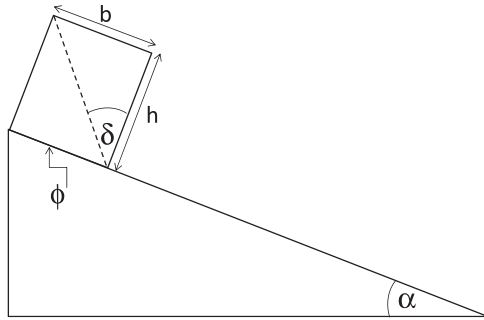


Fig. 1. Sign convention for the block on an inclined plane model used in this paper.

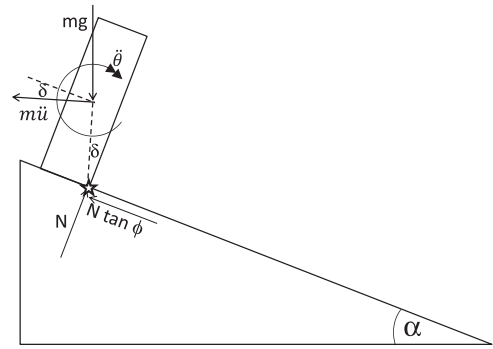


Fig. 4. The dynamics of the block at boundary 4. The block is toppling, hence it has rotational acceleration from which linear acceleration \ddot{u} is derived, and is on the verge of sliding. The rotation hinge is marked with a star; after [7].

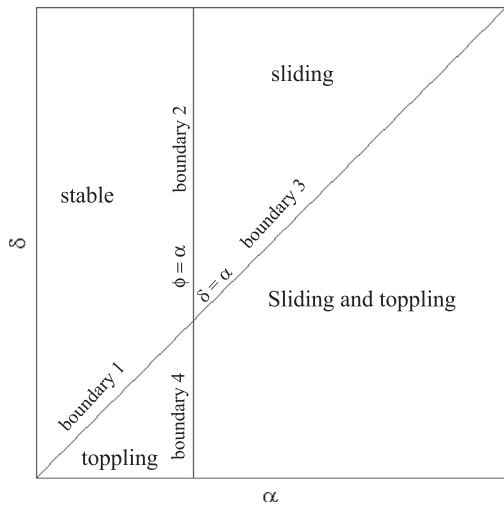


Fig. 2. Kinematic conditions for sliding and toppling for a block on an inclined plane – static analysis; after [1].

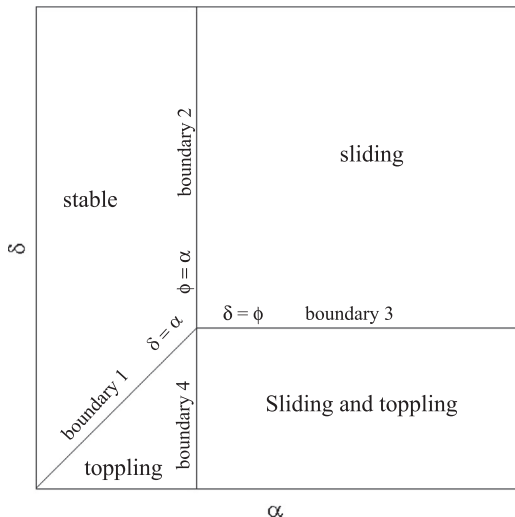


Fig. 3. Kinematic conditions for sliding and toppling with the modified boundary 3; after [4].

results suggest toppling only. This led Yeung [7] to treat boundary 4 as a dynamic boundary as well. The analytical solution for boundary 4 as derived by Yeung [7] is presented in the next paragraph, with incorporation of dynamic effects into the solution.

When a block is on the verge of toppling, the hinge (center of rotation; Fig. 4) tends to move upslope. This movement may prevent sliding, even when permissible by virtue of kinematics, namely when $\phi < \alpha$. Boundary 4 distinguishes between toppling

with and without sliding, therefore the analytical solution derived by Yeung [7] assumes limiting friction ($\phi = \alpha$). Fig. 4 schematically describes the state of forces acting on the block at boundary 4.

The block is under pure rotation, therefore its angular acceleration $\ddot{\theta}$ at the hinge and at the centroid is identical. The forces acting on the block are its weight mg , acting at the centroid, the normal from the incline N , and the limiting friction force $N \tan \phi$, both acting at the hinge. Applying Newton's second law, both parallel and perpendicular to the slope, and taking moments about the centroid of the block, three equations with four variables ($\ddot{\theta}$, \ddot{u} , ϕ and N) can be written as

$$mg \sin \alpha - N \tan \phi = m\ddot{u} \cos \delta \quad (1)$$

$$N - mg \cos \alpha = m\ddot{u} \sin \delta \quad (2)$$

$$N \tan \phi \frac{h}{2} - N \frac{b}{2} = \frac{1}{12} m(h^2 + b^2) \ddot{\theta} \quad (3)$$

The following equation relates $\ddot{\theta}$ and \ddot{u} :

$$\ddot{u} = \frac{1}{2} \ddot{\theta} \sqrt{h^2 + b^2} \quad (4)$$

Solving the set of equations yields the following equation for a friction angle satisfying boundary 4, with any combination of α and δ :

$$\tan \phi = \frac{3 \sin \delta \cos(\alpha - \delta) + \sin \alpha}{3 \cos \delta \cos(\alpha - \delta) + \cos \alpha} \quad (5)$$

or

$$\tan \alpha = \frac{3 \cos^2 \delta \tan \phi - 3 \sin \delta \cos \delta + \tan \phi}{3 \sin^2 \delta - 3 \sin \delta \cos \delta \tan \phi + 1} \quad (6)$$

A modified chart for different modes after correction of boundary 4 for dynamic LEA is presented in Fig. 5 following Yeung [7], for the case of $\phi = 30^\circ$. With the modified boundary 4 Yeung has obtained good agreement between 2D-DDA and the modified kinematic chart.

In a classic paper Goodman and Bray [12] further developed a static LEA solution for the toppling failure of multiple blocks, when the slope is represented by a series of blocks resting on a stepped basal discontinuity. They distinguished between three modes: block toppling, flexural toppling, and both block and flexural toppling. Following Goodman and Bray, flexural toppling and block toppling have been further investigated by many groups, both analytically [13–19], experimentally [13,20] and numerically [16,21,22]. The mode of block slumping has also been studied analytically, experimentally and numerically by [23].

2. Three dimensional visualization of the kinematic mode chart

In the introduction section we have shown that the mode of failure of a single block on an incline depends on three variables: the angles α , ϕ and δ . A three dimensional representation of the mode chart is therefore called for, as presented in Fig. 6. The 3D space, the three axes of which are the three angles, is divided into the four regions of block behavior, namely Mode 1 – stable, Mode 2 – sliding, Mode 3 – sliding and toppling, and Mode 4 – toppling. Consider Fig. 6a, the different failure modes are plotted as follows:

Mode 1, the stable mode, is above the red surface (delineating the $\alpha=\delta$ surface) and to the left of the blue surface (delineating the $\alpha=\phi$ surface).

Mode 2, the sliding mode, is above the green surface (delineating the $\phi=\delta$ surface) and to the right of the blue surface (delineating the $\alpha=\phi$ surface).

Mode 3, the sliding and toppling mode, is below the green surface, indicating the $\phi=\delta$ surface, and in front of the curved surface representing Eq. (6) (note that in this view the curved surface is actually behind the green surface).

Mode 4, or the toppling mode, is below the red surface, indicating $\alpha=\delta$, and behind the curved surface representing Eq. (6).

Fig. 6a presents the 3D space from a point of view similar to those of Figs. 2, 3 and 5 but for different values of ϕ . In Fig. 6b we map the 3D boundaries as viewed from vector $(-1, -1, -1)$. When using $(-1, -1, -1)$ as a viewing vector, vector $(1, 1, 1)$ is reduced to a point, and the surfaces separating the different modes are reduced to lines. With this mapping the 3D space appears as a 2D space where it is easier to perceive the boundaries between the four modes.

3. Adding pseudo-static inertia force to toppling analysis

When trying to determine stability and failure mode under seismic conditions, a common practice in geotechnical engineering is to impose a static force, acting at the centroid of the block in the direction that drives the failure, which simulates the destabilizing effects of an earthquake. Typically, the peak ground acceleration (PGA) of the earthquake record is converted into a pseudo-static horizontal force F acting at the centroid, normalized by the block weight W , and the pseudo-static coefficient k is defined, i.e. $F = kW$. Fig. 7 illustrates the schematics of the block on an incline problem with a horizontal static force F . When adding the pseudo-static force F , a new angle β is introduced, defined here as the angle between the block self-weight W and the resultant of force F and block self-weight W (see Fig. 7), namely:

$$\tan \beta = \frac{F}{W} = k \tag{7}$$

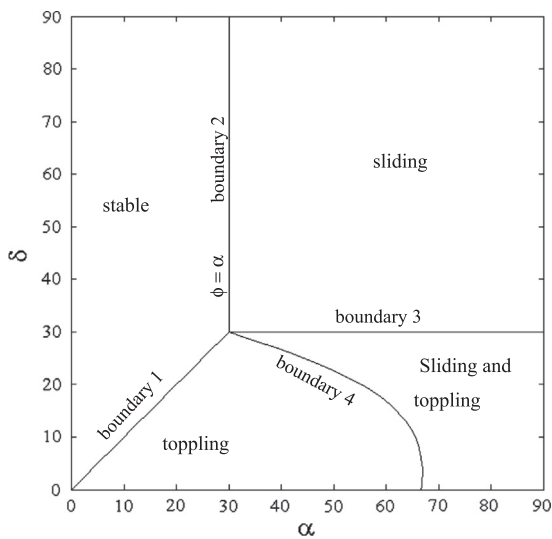


Fig. 5. Kinematic conditions for sliding and toppling with modified boundary 4, for $\phi=30^\circ$; after [7].

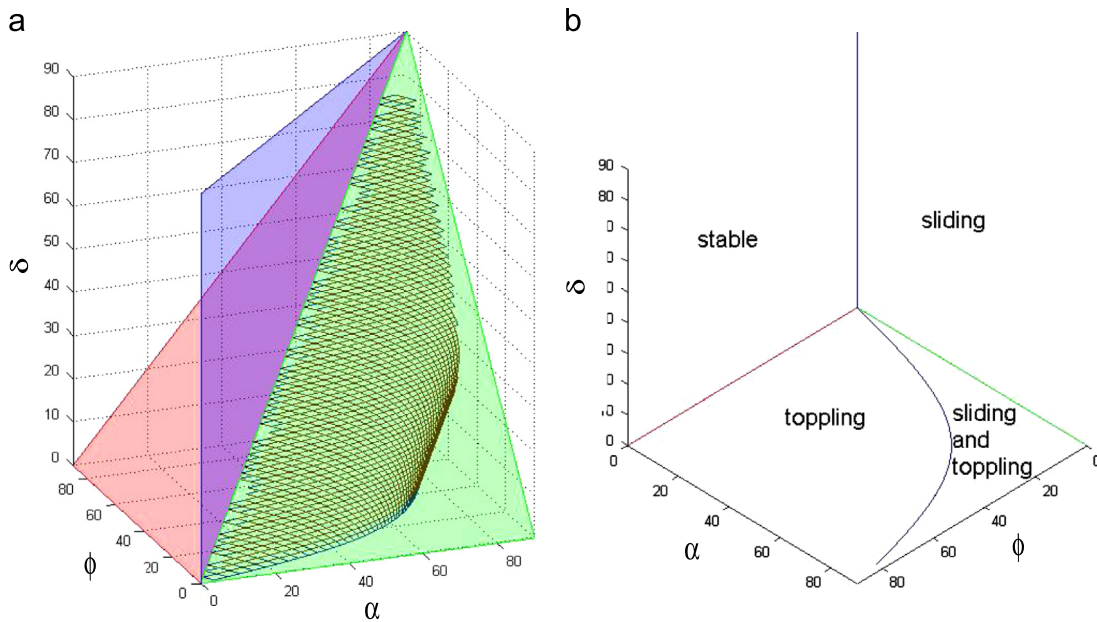


Fig. 6. Kinematic conditions for toppling and sliding. (a) a point of view similar to Figs. 2, 3 and 5. (b) Isometric point of view, viewing vector $(-1, -1, -1)$.

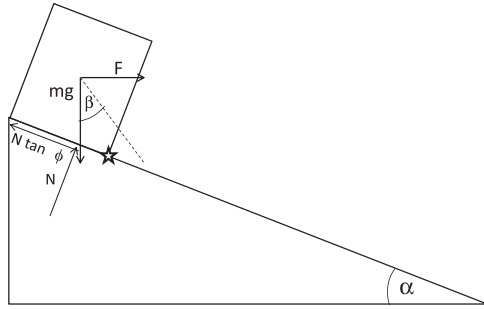


Fig. 7. Force diagram for a block on an incline with pseudo-static force F . The hinge of rotation is marked by a star.

In this section a mode analysis for the block on an incline problem with horizontal force $F = kW$ is derived.

3.1. Boundary 1: between toppling and stable modes

The forces acting on the block at this boundary are W , F , N and the frictional resistance. At the onset of toppling the normal and the frictional forces act at the hinge, therefore they do not contribute to the moments acting on the block. In order for the block to remain stable against toppling, the line of action of the resultant of F and W must pass through the hinge, and so it produces no moments as well. In other words, the stabilizing moments have to be equal to the driving moments at a state of limiting equilibrium

$$\frac{1}{2}bW \cos \alpha = \frac{1}{2}hW \sin \alpha + \frac{1}{2}hF \cos \alpha + \frac{1}{2}bF \sin \alpha \quad (8)$$

Inserting the definition of β into Eq. (8) yields

$$\frac{b}{h} = \frac{\sin \alpha + \cos \alpha \tan \beta}{\cos \alpha - \sin \alpha \tan \beta} = \frac{\tan \alpha + \tan \beta}{1 - \tan \alpha \tan \beta} = \tan(\alpha + \beta) \quad (9)$$

Therefore at the point of limiting equilibrium with respect to toppling

$$\delta = \alpha + \beta \quad (10)$$

If $\delta < \alpha + \beta$, the block will topple. If $\delta > \alpha + \beta$, the block will not topple.

3.2. Boundary 2: between sliding and stable modes

At the point of imminent sliding friction is limiting, therefore the force preventing sliding at the point of limiting equilibrium with respect to sliding is $N \tan \phi$. Force equilibrium parallel to the sliding direction yields

$$N \tan \phi = F \cos \alpha + W \sin \alpha \quad (11)$$

Force equilibrium perpendicular to the sliding direction yields

$$N = W \cos \alpha - F \sin \alpha \quad (12)$$

Inserting Eq. (12) into Eq. (11), and using results from Eq. (9), yields

$$\tan \phi = \frac{F \cos \alpha + W \sin \alpha}{W \cos \alpha - F \sin \alpha} = \frac{\sin \alpha + \cos \alpha \tan \beta}{\cos \alpha - \sin \alpha \tan \beta} = \tan(\alpha + \beta) \quad (13)$$

Therefore the limiting condition for sliding is $\phi = \alpha + \beta$.

3.3. Boundary 3: between sliding and sliding+toppling modes

Bray and Goodman [4] treated boundary 3 as a dynamic one, since the block is both sliding and on the verge of toppling. According to Newton's second law, the force equilibrium in the

downslope direction is

$$F \cos \alpha + W \sin \alpha - N \tan \phi = m\ddot{u} \quad (14)$$

Force equilibrium perpendicular to the slope yields

$$N = W \cos \alpha - F \sin \alpha \quad (15)$$

Finding \ddot{u} from Eqs. (14) and (15), and using Eq. (7), yields

$$\begin{aligned} m\ddot{u} &= F \cos \alpha + W \sin \alpha - \tan \phi (W \cos \alpha - F \sin \alpha) \\ &= W[\tan \beta \cos \alpha + \sin \alpha - \tan \phi (\cos \alpha - \tan \beta \sin \alpha)] \end{aligned} \quad (16)$$

Since the block is on the verge of rotating, the sum of moments about the hinge is (see Fig. 7)

$$\frac{h}{2}F \cos \alpha + \frac{b}{2}F \sin \alpha + \frac{h}{2}W \sin \alpha = \frac{b}{2}W \cos \alpha + \frac{h}{2}m\ddot{u} \quad (17)$$

Substituting Eq. (16) into Eq. (17) yields

$$b/h = \tan \phi \quad \delta = \phi \quad (18)$$

Therefore, the limiting condition for dynamic equilibrium for boundary 3 is $\delta = \phi$.

3.4. Boundary 4: between toppling and sliding+toppling modes

Yeung [7] treated boundary 4 as a dynamic boundary because at this boundary the block is toppling and on the verge of sliding. According to Newton's second law, force equilibrium in the down-slope direction yields

$$F \cos \alpha + W \sin \alpha - N \tan \phi = m\ddot{u} \cos \delta \quad (19)$$

and the force equilibrium perpendicular to the slope yields

$$F \sin \alpha + N - W \cos \alpha = m\ddot{u} \sin \delta \quad (20)$$

Taking moments about the centroid (since at the onset of sliding the angular acceleration is uniform about the block) will again yield Eq. (3). Solving Eqs. (3), (4), (19) and (20) yields

$$\begin{aligned} \tan \phi &= \frac{3 \sin \delta \cos [\delta - (\alpha + \beta)] + \sin(\alpha + \beta)}{3 \cos \delta \cos [\delta - (\alpha + \beta)] + \cos(\alpha + \beta)} \\ &= \frac{3 \sin \delta \cos(\delta - \psi) + \sin \psi}{3 \cos \delta \cos(\delta - \psi) + \cos \psi} \end{aligned} \quad (21)$$

The complete derivation of boundary 4 is provided in the Appendix.

To summarize, in the case where a horizontal force of size $F = kW$ acts on the centroid of the block, the boundaries of the failure modes become a function of three angles: ϕ , δ and $\psi = \alpha + \beta$, instead of α for the case of gravitational loading alone. Alternatively, if using k instead of β is preferable in the definition of ψ , then

$$\psi = \tan^{-1} \frac{k + \tan \alpha}{1 - k \tan \alpha} \quad (22)$$

4. Verification of the dynamic toppling and sliding boundaries with DDA

As mentioned earlier, Yeung [7] verified the 2D-DDA with the analytical solutions of mode analysis under gravitational loading. He found that the 2D-DDA results agreed well with the analytical solution for sliding or toppling and has utilized the DDA results to modify the dynamic boundary between toppling and sliding+toppling (boundary 4). Here we use both 2D and 3D-DDA to verify our pseudo-static analysis which considers an additional inertia force. DDA basics will not be reviewed here; the fundamentals of DDA have been published by Shi and Goodman [11]; for a comprehensive review see [24]. The extension of DDA to three dimensions has been published by Shi [25] and will not be reviewed here either.

Since the 3D-DDA code is relatively new, it has not been extensively verified as the 2D-DDA code. We begin with verification of 3D-DDA using the existing analytical solution for the four failure modes of the block on an incline problem, discussed in Section 4.1. Once verified, we use 2D and 3D-DDA to confirm our modified boundaries which also consider pseudo-static loading, in Sections 4.2 and 4.3, respectively.

The block and the incline are modeled in the DDA, and a measurement point, of which displacements and rotations are documented throughout the simulations, is placed at the hinge (see Fig. 7). The displacements and rotations of the measurement point for the first 0.5 s of the simulation are then examined, and their values determine the nature of the failure mode. It is important to state here that in DDA the rotations are uniform throughout the block, because of the first order approximation.

The following criteria are adopted to judge the obtained failure mode from DDA output:

- The block is considered stable if the recorded displacements at the measurement point are less than 0.001 m and attain stabilization, and if the rotation is less than 0.0001 rad.

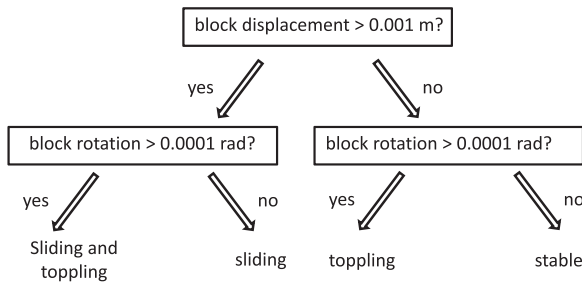


Fig. 8. Flow chart describing criteria for determination of failure mode in numerical simulations.

Table 1 Numerical and physical parameters used for 3D-DDA verification study.

Parameter	Value
Static-dynamic parameter	1 (fully dynamic)
Maximum displacement ratio	0.0001
Maximum time step interval	0.00001 s
Normal contact spring stiffness	1×10^9 N/m
Density	2730 kg/m ³
Young's modulus	42.9 GPa
Poisson's ratio	0.18

Table 2 Numerical and physical parameters used for 2D-DDA verification study by Yeung [7].

Parameter	Value
Static-dynamic parameter	0 (fully static)
Maximum displacement ratio	0.005
Maximum time step interval	0.05 s
Normal contact spring stiffness	1×10^{10} N/m
Density	3000 kg/m ³
Young's modulus	10 GPa
Poisson's ratio	0.49

Table 3 Analytical mode analysis vs. 3D-DDA results for gravitational loading.

α	ϕ	δ	Mode predicted by analytical solution	Mode obtained by DDA
15	20	14	toppling	toppling
15	20	14.4	toppling	toppling
15	20	14.8	toppling	toppling
15	20	15.2	stable	stable
15	20	15.6	stable	stable
15	20	16	stable	stable
15	20	30	stable	stable
15	20	50	stable	stable
15	20	70	stable	stable
40	20	19	sliding+toppling	sliding+toppling
40	20	19.8	sliding+toppling	sliding+toppling
40	20	20.2	sliding	sliding
40	20	21	sliding	sliding
40	20	30	sliding	sliding
14	20	15	stable	stable
14.8	20	15	stable	stable
15.2	20	15	toppling	toppling
15.6	20	15	toppling	toppling
16	20	15	toppling	toppling
30	20	15	toppling	toppling
40	20	15	sliding+toppling	sliding+toppling
50	20	15	sliding+toppling	sliding+toppling
10	20	50	stable	stable
19	20	50	stable	stable
19.8	20	50	stable	stable
20.2	20	50	sliding	stable
20.6	20	50	sliding	stable
21	20	50	sliding	sliding
30	20	50	sliding	sliding
40	20	50	sliding	sliding
50	20	50	sliding	sliding
30	40	30.96	stable	stable
10	20	30.96	stable	stable
50	60	56.31	stable	stable
30	5	11.31	sliding	sliding
10	5	8.53	sliding	sliding
50	45	56.31	sliding	sliding
30	40	11.31	toppling	toppling
10	20	8.53	toppling	toppling
50	60	38.66	toppling	toppling
50	45	38.66	toppling	toppling
30	30	11.3	sliding+toppling	sliding+toppling
10	9	8.53	sliding+toppling	sliding+toppling
22	20	50	sliding	sliding
20.8	20	50	sliding	sliding
15	20	10	toppling	toppling
22	20	10	toppling	toppling
30	20	11.31	toppling	toppling
37	20	11.31	toppling	toppling
37	20	15	toppling	toppling
22	20	18	toppling	toppling

Table 4 Physical and numerical parameters used in the 2D-DDA with external force F.

Parameter	Value
Static-dynamic parameter	1 (fully dynamic)
Maximum displacement ratio	0.001
Maximum time step interval	0.001 s
Normal contact spring stiffness	1×10^{10} N/m
Density	2730 kg/m ³
Young's modulus	42.9 GPa
Poisson's ratio	0.18

- The block is sliding if the displacements are more than 0.001 m and the block accelerates, and if the rotation is less than 0.0001 rad.

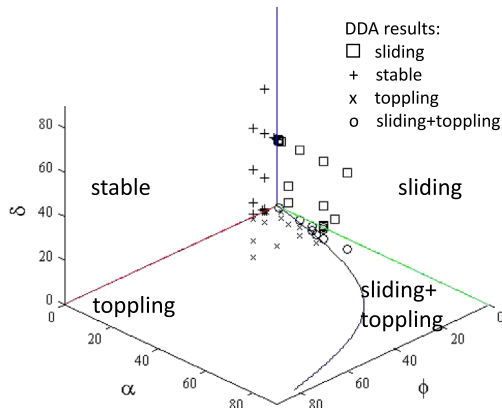


Fig. 9. Results of 3D-DDA verification analysis with the analytical solution.

- The block is toppling if the displacements are less than 0.001 m, but the rotation is more than 0.0001 rad.
- The block is sliding and toppling if both the displacement is larger than 0.001 m and the rotation is larger than 0.0001 rad.

A flow chart describing the failure mode judgment criteria for DDA output is presented in Fig. 8. The numerical control parameters used in the DDA verification are provided in Tables 1 and 4.

4.1. Verification of 3D-DDA with mode analysis charts under gravitational loading

The numerical and physical parameters used in the verification study of the 3D-DDA are presented in Table 1. For the sake of comparison with the original verification study performed by Yeung [7] the control parameters used in his analysis are provided in Table 2. As can be observed from Tables 1 and 2, the density and Young's modulus are of the same order of magnitude, whereas the time step interval and the normal contact spring stiffness in 3D-DDA are three and one orders of magnitude lower, respectively. The friction angle selected for the study was 20° in most analyses. The list of analyses performed in the verification study is provided in Table 3. Projection of the results on the three-dimensional mode chart is presented in Fig. 9. The agreement between the 3D-DDA and the analytical solution is excellent.

4.2. Verification of the mode analysis charts with 2D-DDA for pseudo-static force

The 2D-DDA has been verified many times in the past, and has proved to be a useful and reliable tool for numerical modeling of discontinuous problems in geomechanics and rock mechanics [26–28]. Therefore we use the 2D-DDA to confirm the analytical solution derived for a block on an incline subjected to gravity and a horizontal pseudo-static force. The physical and numerical parameters used in the 2D-DDA simulations are presented in Table 4. The time step size that can be used in the 2D-DDA is 100 times larger than the one used in 3D-DDA.

Since the addition of an external force F introduces a new angle to the mode chart, the angle $\psi = \alpha + \beta$, different values for ψ can be generated by changing β (through a change in F) without changing α . This allows for fast modeling and multiple simulations using the same DDA mesh. The α used in the verification study was 10°. Table 5 lists the different simulations and their results for the 2D-DDA verification.

Fig. 10 presents the results of the 2D-DDA simulations with external force F in the ψ , ϕ and δ space. Note the excellent agreement between the numerical DDA and analytical solutions. As mentioned before, DDA simulation were performed with a fixed

Table 5 Analytical mode analysis vs. 2D-DDA with horizontal force F .

$\psi(\alpha + \beta)$	ϕ	δ	Mode predicted by analytical solution	Mode obtained by DDA
29	35	30.96	stable	stable
29.5	35	30.96	stable	stable
30	35	30.96	stable	stable
30.5	35	30.96	stable	stable
30.9	35	30.96	stable	stable
31	35	30.96	toppling	toppling
31.5	35	30.96	toppling	toppling
32	35	30.96	toppling	toppling
32.5	35	30.96	toppling	toppling
30	50	30.96	stable	stable
30.5	50	30.96	stable	stable
30.9	50	30.96	stable	stable
31	50	30.96	toppling	toppling
31.5	50	30.96	toppling	toppling
32.5	50	30.96	toppling	toppling
18	20	30.96	stable	stable
18.5	20	30.96	stable	stable
19	20	30.96	stable	stable
19.5	20	30.96	stable	stable
19.8	20	30.96	stable	stable
20.2	20	30.96	sliding	sliding
21	20	30.96	sliding	sliding
21.5	20	30.96	sliding	sliding
22	20	30.96	sliding	sliding
48	50	30.96	toppling	toppling
49.8	50	30.96	toppling	toppling
52	50	30.96	toppling	toppling
35	30	30.96	sliding	sliding + toppling
36	30	30.96	sliding	sliding
35	29	30.96	sliding	sliding
35	25	30.96	sliding	sliding
40	30	30.96	sliding	sliding
45	30	30.96	sliding	sliding
50	30	30.96	sliding	sliding
60	30	30.96	sliding	sliding
70	30	30.96	sliding	sliding
80	20	30.96	sliding	sliding
85	40	30.96	sliding + toppling	sliding + toppling
66	40	30.96	sliding + toppling	sliding + toppling
64	40	30.96	sliding + toppling	sliding + toppling
62	40	30.96	toppling	toppling
80	40	30.96	sliding + toppling	sliding + toppling
82	50	30.96	toppling	toppling
84	50	30.96	toppling	sliding + toppling
86	50	30.96	sliding + toppling	sliding + toppling
80	60	30.96	toppling	toppling
70	10	30.96	sliding	sliding
70	20	30.96	sliding	sliding
70	40	30.96	sliding + toppling	sliding + toppling
70	50	30.96	toppling	toppling
20	21	20.30	stable	toppling
20	21	30.96	stable	stable
20	21	40.03	stable	stable
20	21	50.19	stable	stable
20	21	60.11	stable	stable
20	21	71.57	stable	stable
20	19	20.30	sliding	sliding
20	19	30.96	sliding	sliding
20	19	40.03	sliding	sliding
20	19	50.19	sliding	sliding
20	18.9	60.11	sliding	sliding
20	19	71.57	sliding	sliding
20	80	20.30	stable	stable
30	80	30.96	stable	stable
40	80	40.70	stable	stable
50	80	50.19	stable	stable
60	80	60.40	stable	stable
70	80	70.35	stable	stable
20	80	19.80	toppling	toppling
30	80	29.25	toppling	toppling
40	80	39.35	toppling	toppling
50	80	49.24	toppling	toppling
60	80	59.53	toppling	toppling
70	80	69.68	toppling	toppling

Table 5 (continued)

$\psi(\alpha+\beta)$	ϕ	δ	Mode predicted by analytical solution	Mode obtained by DDA
10	5.8	6.84	sliding	sliding
20	6	6.84	sliding	sliding
30	16	16.70	sliding	sliding
40	26	26.57	sliding	sliding
50	35	35.75	sliding	sliding
60	43	43.53	sliding	sliding
70	54	54.46	sliding	sliding
80	63	63.43	sliding	sliding
10	8	6.84	sliding + toppling	sliding + toppling
20	8	6.84	sliding + toppling	sliding + toppling
30	17	16.70	sliding + toppling	sliding + toppling
40	27	26.57	sliding + toppling	sliding + toppling
50	36	35.75	sliding + toppling	sliding + toppling
60	44	43.53	sliding + toppling	sliding + toppling
70	55	54.46	sliding + toppling	sliding + toppling
80	64	63.43	sliding + toppling	sliding + toppling
20	10	7.07	sliding + toppling	sliding + toppling
30	20	17.22	sliding + toppling	sliding + toppling
40	20	12.95	sliding + toppling	sliding + toppling
50	20	7.07	sliding + toppling	sliding + toppling
60	40	33.02	sliding + toppling	sliding + toppling
70	50	42.92	sliding + toppling	sliding + toppling
80	62	53.06	toppling	sliding + toppling
20	10	6.05	toppling	toppling
30	20	16.17	toppling	toppling
40	20	11.97	toppling	toppling
50	20	6.05	toppling	toppling
60	40	32.05	toppling	toppling
70	50	41.99	toppling	toppling
80	62	52.00	toppling	toppling
18	30	29.00	stable	stable
50	30	29.00	sliding + toppling	sliding + toppling
40	30	29.00	sliding + toppling	sliding + toppling
35	30	29.00	sliding + toppling	sliding + toppling
32	30	29.00	toppling	toppling
50	35	29.00	toppling	toppling

Table 6

Analytical mode analysis vs. 3D-DDA with horizontal force F .

$\psi(\alpha+\beta)$	ϕ	δ	Mode predicted by analytical solution	Mode obtained by DDA
29	80	30.96	stable	stable
29.5	80	30.96	stable	stable
30	80	30.96	stable	stable
30.5	80	30.96	stable	stable
30.9	80	30.96	stable	stable
31	80	30.96	toppling	toppling
31.5	80	30.96	toppling	toppling
32	80	30.96	toppling	toppling
32.5	80	30.96	toppling	toppling
33	80	30.96	toppling	toppling
27	28	30.96	stable	stable
27.5	28	30.96	stable	stable
27.8	28	30.96	stable	stable
28.2	28	30.96	sliding	sliding
28.5	28	30.96	sliding	sliding
29	28	30.96	sliding	sliding
60	40	30.96	toppling	toppling
60.5	40	30.96	toppling	toppling
61	40	30.96	toppling	toppling
61.5	40	30.96	toppling	toppling
62	40	30.96	toppling	toppling
62.5	40	30.96	toppling	toppling
63	40	30.96	toppling	toppling
63.5	40	30.96	sliding + toppling	sliding + toppling
64	40	30.96	sliding + toppling	sliding + toppling
64.5	30	30.96	sliding + toppling	sliding + toppling
65	30	30.96	sliding + toppling	sliding + toppling
65.5	30	30.96	sliding + toppling	sliding + toppling
55	30	30.96	sliding	sliding
55	30	30.54	sliding	sliding
55	30	30.11	sliding	sliding
55	30	29.68	sliding + toppling	sliding + toppling
55	50	19.80	toppling	toppling
20	21	20.30	toppling	toppling
20	21	30.96	stable	stable
20	21	40.03	stable	stable
20	21	50.19	stable	stable
20	21	60.11	stable	stable
20	21	71.57	stable	stable
20	19	20.30	sliding	sliding
20	19	30.96	sliding	sliding
20	19	40.03	sliding	sliding
20	19	50.19	sliding	sliding
20	19	60.11	sliding	sliding
20	19	71.57	sliding	sliding
30	80	20.30	stable	stable
40	80	30.96	stable	stable
50	80	40.70	stable	stable
60	80	50.19	stable	stable
70	80	60.40	stable	stable
80	80	70.35	stable	stable
20	80	19.80	toppling	toppling
30	80	29.25	toppling	toppling
40	80	39.35	toppling	toppling
50	80	49.24	toppling	toppling
60	80	59.53	toppling	toppling
70	80	69.68	toppling	toppling
10	5.8	6.84	sliding	sliding
20	6	6.84	sliding	sliding
30	16	16.70	sliding	sliding
40	26	26.57	sliding	sliding
50	35	35.75	sliding	sliding
60	43	43.53	sliding	sliding
70	54	54.46	sliding	sliding
80	63	63.43	sliding	sliding
10	8	6.84	sliding + toppling	sliding + toppling
20	8	6.84	sliding + toppling	sliding + toppling
30	17	16.70	sliding + toppling	sliding + toppling
40	27	26.57	sliding + toppling	sliding + toppling
50	36	35.75	sliding + toppling	sliding + toppling
60	44	43.53	sliding + toppling	sliding + toppling
70	55	54.46	sliding + toppling	sliding + toppling
80	64	63.43	sliding + toppling	sliding + toppling
20	10	7.07	sliding + toppling	sliding + toppling

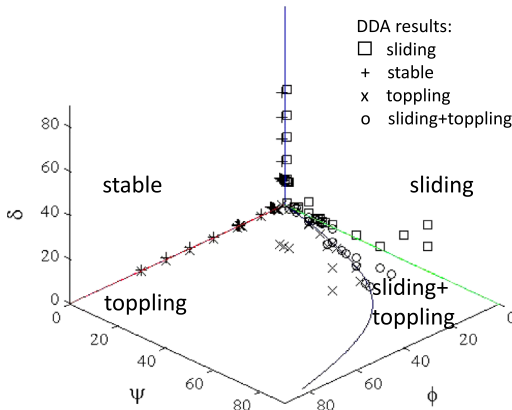


Fig. 10. Results of 2D-DDA verification analysis with the analytical solution, with the application of external force.

inclination angle of 10°, and the angle ψ was altered by the force F . A few simulations were performed with different inclination angles, to make sure results of the simulations are repeated.

4.3. Verification of the mode analysis charts with 3D-DDA for pseudo-static force

A similar process of verification was performed with the 3D-DDA. The physical and numerical control parameters are identical to the ones used in the gravitational loading verification in Section 4.1, and are listed in Table 1. The analyses performed in this section are listed in Table 6, and results are plotted in Fig. 11.

Table 6 (continued)

$\psi(\alpha+\beta)$	ϕ	δ	Mode predicted by analytical solution	Mode obtained by DDA
30	20	17.22	sliding+toppling	sliding+toppling
40	20	12.95	sliding+toppling	sliding+toppling
50	20	7.07	sliding+toppling	sliding+toppling
60	40	33.02	sliding+toppling	sliding+toppling
70	50	42.92	sliding+toppling	sliding+toppling
80	62	53.06	sliding+toppling	sliding+toppling
20	10	6.05	toppling	toppling
30	20	16.17	toppling	toppling
40	20	11.97	toppling	toppling
50	20	6.05	toppling	toppling
60	40	32.05	toppling	toppling
70	50	41.99	toppling	toppling
80	62	52.00	toppling	toppling
30	80	30.96	stable	stable
30	80	29.25	toppling	toppling

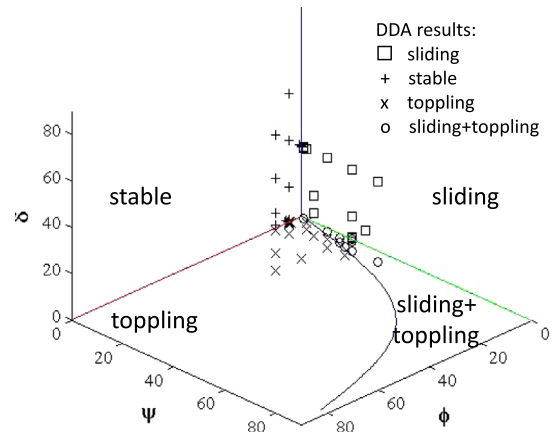


Fig. 11. Results of 3D-DDA verification analysis with the analytical solution, with the application of external force.

Note the good agreement between the analytical solution and the 3D-DDA.

5. Discussion

To demonstrate the applicability of the newly incorporated pseudo-static force in the failure mode chart for block on an inclined plane, two cases of blocks with different geometries are presented (Fig. 12), and the failure modes are calculated analytically. In the first example, a block of height=1 m and width=1.19 m ($\delta=50^\circ$) is resting on a plane inclined at $\alpha=10^\circ$. The friction of the interface is $\phi=30^\circ$. Let us examine the mode of the block as a function of the k value, i.e. the pseudo-static coefficient. As explained earlier, a change in k will lead to a change in β , which in turn will change the value of ψ . We start with a k value of 0, increase it by intervals of 0.1, up to 0.8, and plot the combination of the three angles, δ , ϕ and ψ , for the changing values of k on the three-dimensional plot (square symbols in Fig. 12). For k values from 0 (no pseudo-static force) to 0.3, the block remains in the stable region. For values of $k \geq 0.4$, the combination of angles shifts the block to the sliding region. This means that for the described set of angles, k value of 0.4 and greater would cause the block to fail in sliding. In the second example, a block of height=1 m and width=0.27 m ($\delta=15^\circ$) is resting on the same incline as in the previous example (Fig. 12). For $k=0$, the block is at rest. Increasing k to 0.1 is sufficient to cause toppling, and the block will shift to the mode of sliding+toppling when k exceeds the value of 1.35 (\times symbols in Fig. 12). These two examples clearly demonstrate how by simple calculations, our new mode chart can be used in order to predict the mode of failure of a block on an incline, when subjected to a pseudo-static force.

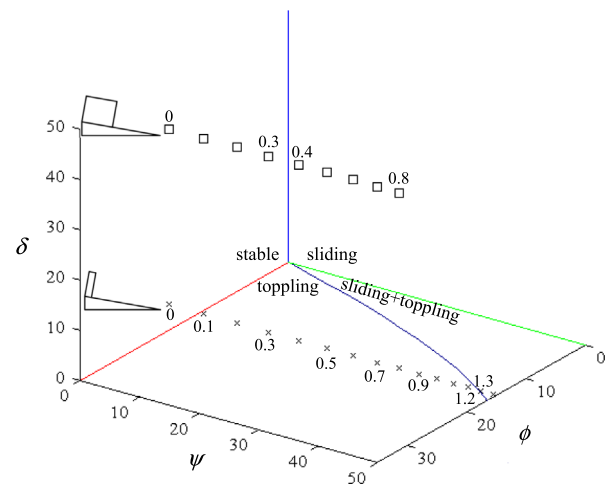


Fig. 12. Mode analysis for two block geometries: $\delta=50^\circ$ (square symbols) and $\delta=15^\circ$ (\times symbols). For both geometries $\alpha=10^\circ$ and $\phi=30^\circ$. The mode of the block changes with changing value of k , the pseudo-static coefficient, denoted near the symbols.

Now one may ask: why is pre-knowledge of the exact failure mode required? In order to demonstrate the importance of determining the failure mode of a block before a design strategy is decided, two simulations were performed using the 2D-DDA, with $k=0$, for simplicity. The model used in the simulations is presented in Fig. 13. The model consists of a fixed base block, inclined at $\alpha=25^\circ$, a fixed back wall representing the rock mass, and a block which is kinematically free to move (see Fig. 13). The block angle, δ , is 22° . The block is anchored to the back wall by three identical horizontal rock bolts (Fig. 13). The stiffness of the rock bolts is 321.7 MN/m. In the first simulation, the friction angle ϕ is set to 15° , a value that puts the block in the sliding mode. In the second simulation, ϕ is set to 30° , which puts the block in the toppling mode. The physical and numerical control parameters used in these simulations are listed in Table 4. In Fig. 14 the bolt forces are plotted, for the two different simulations. As can be observed from Fig. 14, when the block is sliding the forces that develop at the different bolts are very similar, with differences of up to

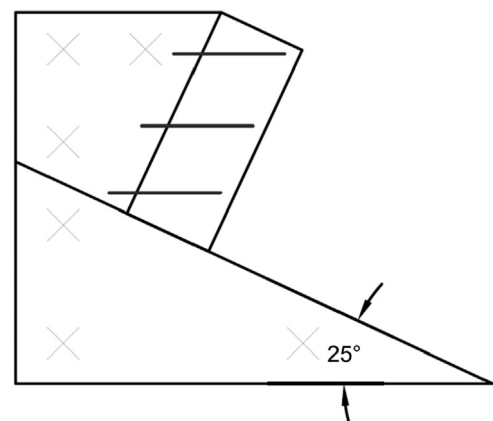


Fig. 13. The model used for the rock bolt force simulations.

5%. When the block is toppling however, there is a great difference between the forces that develop in the different bolts, for example, 250% difference between the top bolt and the bottom one. This way, when designing the support scheme for toppling failure, the engineer can use shorter bolts for the bottom part, and long ones for the top, while when designing support for sliding mode, similar bolt lengths should be used at all slope heights. This demonstrates how

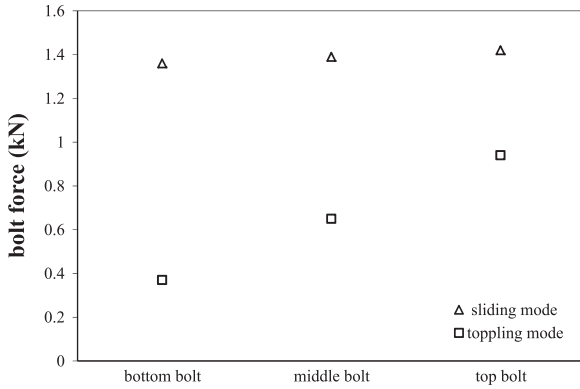


Fig. 14. The forces developed at the rock bolts for the two simulations. Triangular symbols: $\phi=15^\circ$, the block is sliding. Square symbols: $\phi=30^\circ$, the block is toppling.

determining the failure mode of a block, both under static and pseudo-static conditions, can greatly assist the engineer in designing the most efficient support and stabilizing method.

6. Summary and conclusions

In this paper, we first review previous research regarding the failure mode analysis for the problem of a block on an incline. We plot, for the first time, the four possible modes (stability, sliding, sliding+toppling and toppling) in a three dimensional space, as the modes are a function of three angles: the block angle δ (block width/block height), the friction angle of the interface between the slope and the block ϕ , and the inclination of the slope α . We then derive a new failure mode chart, incorporating the frequently used pseudo-static approach. We verify the numerical 3D-DDA code with mode analysis for gravitational loading, and then confirm the pseudo-static mode chart, derived in this paper, with the 2D and 3D-DDA.

In the new chart, derived in this paper, the mode of failure of the block is again a function of three angles: δ , ϕ , and a new angle, $\psi=\alpha+\beta$, where β is the angle between the resultant of the block weight and the pseudo-static force applied on the block, and the vertical direction. Verification of the 3D-DDA with the formerly derived analytical solution for a block on an inclined plane under gravitational loading alone proves the 3D-DDA can accurately solve the problem. Furthermore, the 2D and 3D-DDA simulations of the block subjected to pseudo-static horizontal force confirm the new analytical boundaries derived here, and once again confirm the dynamic nature of boundary 4, which separates toppling from sliding and toppling.

When designing reinforcement for rock slopes that are susceptible for either sliding or toppling failure modes, it is crucial to take into account seismic forces that can affect the stability of the rock mass. The new chart for failure modes, with the incorporation of a pseudo-static horizontal force simulating the seismic force of an earthquake, is an easy, more intuitive way to understand and predict the behavior of rock masses subjected to seismic forces, when those are modeled as a pseudo-static horizontal force. When using the new chart, the pseudo-static force for the mode analysis should be carefully selected, taking into account seismic hazard assessments in the region discussed, and preferably site effects, where these are known.

Acknowledgments

This study is funded by Israel Science Foundation through Grant ISF-2201, Contract no. 556/08.

Appendix. Derivation of boundary 4: between toppling and sliding+toppling

For boundary 4, which is a dynamic boundary between toppling and toppling with sliding, the block is toppling, and on the verge of sliding, i.e. friction is limiting. There are four unknown variables $\{N, \phi, \ddot{u}, \text{ and } \dot{\theta}\}$, and so four equations must be derived. Forces in the downslope direction

$$F \cos \alpha + W \sin \alpha = N \tan \phi + m \ddot{u} \cos \delta \tag{A.1}$$

Forces perpendicular to slope

$$F \sin \alpha + N = W \cos \alpha + m \ddot{u} \sin \delta \tag{A.2}$$

Moments about the centroid

$$\frac{1}{2} N h \tan \phi = \frac{1}{2} N b + \frac{1}{12} m (h^2 + b^2) \ddot{\theta} \tag{A.3}$$

And the relationship between the linear acceleration and rotational acceleration

$$\ddot{u} = \frac{1}{2} \ddot{\theta} \sqrt{h^2 + b^2} \tag{A.4}$$

Remembering that

$$h^2 + b^2 = h^2 \left(1 + \frac{b^2}{h^2} \right) = h^2 (1 + \tan^2 \delta) = \frac{h^2}{\cos^2 \delta} \tag{A.5}$$

Eq. (A.4) can be re-written as

$$\ddot{u} = \frac{\ddot{\theta} h}{2 \cos \delta} \tag{A.6}$$

$$\ddot{\theta} = \frac{2 \ddot{u} \cos \delta}{h} \tag{A.7}$$

Inserting Eq. (A.7) into Eq. (A.3)

$$N(h \tan \phi - b) = \frac{m}{6} \frac{h^2}{\cos^2 \delta} \frac{2 \ddot{u} \cos \delta}{h} = \frac{m h \ddot{u}}{3 \cos \delta} \tag{A.8}$$

$$\begin{aligned} m \ddot{u} &= N \frac{3 \cos \delta (h \tan \phi - b)}{h} = 3 N \cos \delta \left(\tan \phi - \frac{b}{h} \right) \\ &= 3 N \cos \delta (\tan \phi - \tan \delta) \end{aligned} \tag{A.9}$$

Remembering that $F = W \tan \beta$, and inserting Eq. (A.9), Eq. (A.1) becomes

$$\begin{aligned} W \tan \beta \cos \alpha + W \sin \alpha &= N [\tan \phi + 3 \cos^2 \delta (\tan \phi - \tan \delta)] \\ N &= \frac{W (\tan \beta \cos \alpha + \sin \alpha)}{\tan \phi + 3 \cos^2 \delta (\tan \phi - \tan \delta)} \end{aligned} \tag{A.10}$$

Inserting Eqs. (A.10) and (A.9) into Eq. (A.2) yields

$$\begin{aligned} W \tan \beta \sin \alpha + \frac{W (\tan \beta \cos \alpha + \sin \alpha)}{\tan \phi + 3 \cos^2 \delta (\tan \phi - \tan \delta)} \\ = W \cos \alpha + \frac{3 W (\tan \beta \cos \alpha + \sin \alpha) \sin \delta \cos \delta (\tan \phi - \tan \delta)}{\tan \phi + 3 \cos^2 \delta (\tan \phi - \tan \delta)} \end{aligned} \tag{A.11}$$

Finding a common denominator and eliminating it on both sides of the equation yields

$$\begin{aligned} 3 \sin \alpha \cos^2 \delta (\tan \phi - \tan \delta) \tan \beta + \sin \alpha \tan \phi \tan \beta \\ + \sin \alpha + \cos \alpha \tan \beta \\ = 3 \cos \alpha \cos^2 \delta (\tan \phi - \tan \delta) + \cos \alpha \tan \phi \\ + 3 \sin \delta \cos \delta (\cos \alpha \tan \beta + \sin \alpha) (\tan \phi - \tan \delta) \end{aligned} \tag{A.12}$$

The left hand side of Eq. (A.12) becomes

$$\begin{aligned} \tan \phi (\sin \alpha \tan \beta + 3 \sin \alpha \cos^2 \delta \tan \beta) \\ - 3 \sin \alpha \sin \delta \cos \delta \tan \beta + \cos \alpha \tan \beta + \sin \alpha \end{aligned}$$

The right hand side of Eq. (A.12) becomes

$$\begin{aligned} & \tan \phi (3 \cos \alpha \cos^2 \delta + \cos \alpha + 3 \sin \delta \cos \delta \cos \alpha \tan \beta \\ & + 3 \sin \delta \cos \delta \sin \alpha) \\ & - 3 \cos \alpha \sin \delta \cos \delta - 3 \sin^2 \delta \cos \alpha \tan \beta - 3 \sin^2 \delta \sin \alpha \end{aligned}$$

Combining from both sides of Eq. (A.12) all the expressions multiplied by $\tan \phi$ gives

$$\begin{aligned} & 3 \sin \alpha \tan \beta \cos^2 \delta + \sin \alpha \tan \beta - 3 \sin \delta \cos \delta \sin \alpha \\ & - 3 \sin \delta \cos \delta \cos \alpha \tan \beta \\ & - 3 \cos \alpha \cos^2 \delta - \cos \alpha \end{aligned}$$

Multiply by $\cos \beta$

$$\begin{aligned} & 3 \sin \alpha \sin \beta \cos^2 \delta + \sin \alpha \sin \beta - 3 \sin \delta \cos \delta \sin \alpha \cos \beta \\ & - 3 \sin \delta \cos \delta \cos \alpha \sin \beta - 3 \cos \alpha \cos^2 \delta \cos \beta \\ & - \cos \alpha \cos \beta = 3 \cos^2 \delta (\sin \alpha \sin \beta - \cos \alpha \cos \beta) \\ & - 3 \sin \delta \cos \delta (\sin \alpha \cos \beta + \cos \alpha \sin \beta) + \sin \alpha \sin \beta \\ & - \cos \alpha \cos \beta = -3 \cos^2 \delta \cos(\alpha + \beta) \\ & - 3 \sin \delta \cos \delta \sin(\alpha + \beta) - \cos(\alpha + \beta) \end{aligned}$$

Combine from both sides of Eq. (A.12) all the expressions that are not multiplied by $\tan \phi$

$$\begin{aligned} & 3(\sin \alpha \tan \beta \sin \delta \cos \delta - \sin^2 \delta \sin \alpha - \sin^2 \delta \cos \alpha \tan \beta \\ & - \cos \alpha \sin \delta \cos \delta) \\ & - \sin \alpha - \cos \alpha \tan \beta \end{aligned}$$

Multiplying by $\cos \beta$

$$\begin{aligned} & 3(\sin \alpha \sin \beta \sin \delta \cos \delta - \sin^2 \delta \sin \alpha \cos \beta - \sin^2 \delta \cos \alpha \sin \beta \\ & - \cos \alpha \sin \delta \cos \delta \cos \beta) \\ & - \sin \alpha \cos \beta - \cos \alpha \sin \beta = 3[\sin \delta \cos \delta (\sin \alpha \sin \beta \\ & - \cos \alpha \cos \beta) - \sin^2 \delta (\sin \alpha \cos \beta + \cos \alpha \sin \beta)] \\ & - \sin \alpha \cos \beta - \cos \alpha \sin \beta = 3[-\sin \delta \cos \delta \cos(\alpha + \beta) \\ & - \sin^2 \delta \sin(\alpha + \beta)] - \sin(\alpha + \beta) \end{aligned}$$

Combine both expressions

$$\begin{aligned} \tan \phi &= \frac{3[\sin \delta \cos \delta \cos(\alpha + \beta) + \sin^2 \delta \sin(\alpha + \beta)] + \sin(\alpha + \beta)}{3[\sin \delta \cos \delta \sin(\alpha + \beta) + \cos^2 \delta \cos(\alpha + \beta)] + \cos(\alpha + \beta)} \\ &= \frac{3 \sin \delta [\cos \delta \cos(\alpha + \beta) + \sin \delta \sin(\alpha + \beta)] + \sin(\alpha + \beta)}{3 \cos \delta [\cos \delta \cos(\alpha + \beta) + \sin \delta \sin(\alpha + \beta)] + \cos(\alpha + \beta)} \end{aligned} \quad (A.13)$$

And finally

$$\tan \phi = \frac{3 \sin \delta \cos [\delta - (\alpha + \beta)] + \sin(\alpha + \beta)}{3 \cos \delta \cos [\delta - (\alpha + \beta)] + \cos(\alpha + \beta)} \quad (A.14)$$

References

- [1] Ashby J.P. Sliding and toppling modes of failure in models and jointed rock slopes. MSc thesis. Imperial College; 1971.
- [2] Hoek E, Bray JW. Rock slope engineering. London: The Institution of Mining and Metallurgy; 1977.
- [3] Voegele M.D. Rational design of tunnel supports: an interactive graphics based analysis of the support requirements of excavations in jointed rock masses. PhD thesis. Department of Civil and Mineral Engineering, University of Minnesota; 1979.
- [4] Bray JW, Goodman RE. The theory of base friction models. International Journal of Rock Mechanics and Mining Sciences 1981;18:453–68.
- [5] Yu Z, Ishijima Y, Sato M. Distinct element method – application to analyse sliding and toppling failures. Nonferrous Metals 1987;39:1–11.
- [6] Sagaseta C. On the modes of instability of a rigid block on an inclined plane. Rock Mechanics and Rock Engineering 1986;19:261–6.
- [7] Yeung M.R. Application of Shi's Discontinuous Deformation Analysis to the study of rock behavior. PhD thesis. Department of Civil Engineering, Berkeley: University of California; 1991.
- [8] Shi G. Discontinuous Deformation Analysis – a new numerical method for the statics and dynamics of block system. PhD thesis. Department of Civil Engineering, Berkeley: University of California; 1988.
- [9] Shi G. Block system modeling by Discontinuous Deformation Analysis. Southampton: Computational Mechanics Publications; 1993.
- [10] Shi G-H, Goodman RE. Two dimensional Discontinuous Deformation Analysis. International Journal for Numerical and Analytical Methods in Geomechanics 1985;9:541–56.
- [11] Shi G-H, Goodman RE. Generalization of two dimensional Discontinuous Deformation Analysis for forward modelling. International Journal for Numerical and Analytical Methods in Geomechanics 1989;13:359–80.
- [12] Goodman R.E., Bray J.W. Toppling of rock slopes. In: Proceedings of the specialty conference on rock engineering for foundations and slopes. Boulder, Colorado: American Society of Civil Engineers; 1976. p. 201–34.
- [13] Amini M, Majdi A, Aydan O. Stability analysis and the stabilisation of flexural toppling failure. Rock Mechanics and Rock Engineering 2009;42:751–82.
- [14] Amini M, Majdi A, Veshadi MA. Stability analysis of rock slopes against block-flexure toppling failure. Rock Mechanics and Rock Engineering 2012;45:519–32.
- [15] Aydan O, Kawamoto T. The stability of slopes and underground openings against flexural toppling and their stabilization. Rock Mechanics and Rock Engineering 1992;25:143–65.
- [16] Bobet A. Analytical solutions for toppling failure. International Journal of Rock Mechanics and Mining Sciences 1999;36:971–80.
- [17] Liu CH, Jaksa MB, Meyers AG. Improved analytical solution for toppling stability analysis of rock slopes. International Journal of Rock Mechanics and Mining Sciences 2008;45:1361–72.
- [18] Majdi A, Amini M. Analysis of geo-structural defects in flexural toppling failure. International Journal of Rock Mechanics and Mining Sciences 2011;48:175–86.
- [19] Sagaseta C, Sanchez JM, Canizal J. A general analytical solution for the required anchor force in rock slopes with toppling failure. International Journal of Rock Mechanics and Mining Sciences 2001;38:421–35.
- [20] Adhikary DP, Dyskin AV, Jewell RJ, Stewart DP. A study of the mechanism of flexural toppling failure of rock slopes. Rock Mechanics and Rock Engineering 1997;30:75–93.
- [21] Brideau MA, Stead D. Controls on block toppling using a three-dimensional distinct element approach. Rock Mechanics and Rock Engineering 2010;43:241–60.
- [22] Scholtes L, Donze FV. Modelling progressive failure in fractured rock masses using a 3D discrete element method. International Journal of Rock Mechanics and Mining Sciences 2012;52:18–30.
- [23] Kieffer S.D. Rock Slumping – a compound failure mode of jointed hard rock slopes. PhD thesis. Department of Civil and Environmental Engineering, Berkeley: University of California; 1998.
- [24] Jing LR. Formulation of discontinuous deformation analysis (DDA) – an implicit discrete element model for block systems. Engineering Geology 1998;49:371–81.
- [25] Shi G. Three dimensional discontinuous deformation analyses. In: Proceedings of the 38th US rock mechanics symposium. Washington, DC; 2001. p. 1421–8.
- [26] Kamai R, Hatzor YH. Numerical analysis of block stone displacements in ancient masonry structures: a new method to estimate historic ground motions. International Journal for Numerical and Analytical Methods in Geomechanics 2008;32:1321–40.
- [27] MacLaughlin MM, Doolin DM. Review of validation of the discontinuous deformation analysis (DDA) method. International Journal for Numerical and Analytical Methods in Geomechanics 2006;30:271–305.
- [28] Yagoda-Biran G, Hatzor YH. Constraining paleo PGA values by numerical analysis of overturned columns. Earthquake Engineering and Structural Dynamics 2010;39:462–72.